IEEE Photonics Journal
An IEEE Photonics Society Publication

Open Access

Maximal Acceptable Ghost Images for Designing a Legible Windshield-Type Vehicle Head-Up Display

Volume 9, Number 6, December 2017

Zong Qin
Fang-Cheng Lin
Yi-Pai Huang
Han-Ping D. Shieh, ***Fellow, IEEE***

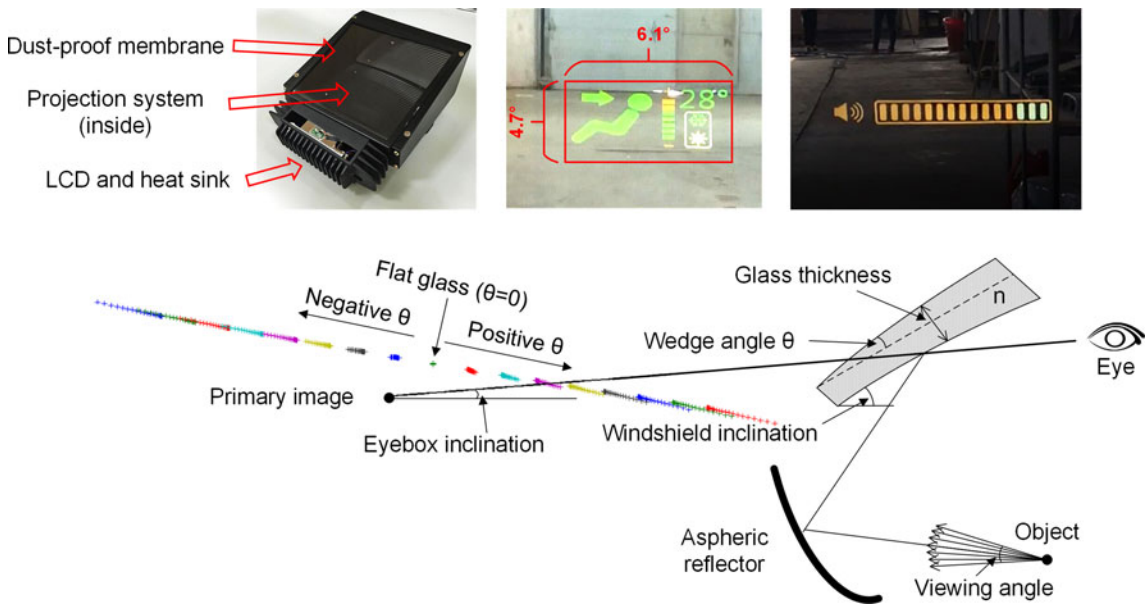

DOI: 10.1109/JPHOT.2017.2758820
1943-0655

Maximal Acceptable Ghost Images for Designing a Legible Windshield-Type Vehicle Head-Up Display

Zong Qin, Fang-Cheng Lin, Yi-Pai Huang, and Han-Ping D. Shieh, *Fellow, IEEE*

Department of Photonics and Display Institute, National Chiao Tung University, Hsinchu 300, Taiwan, R.O.C.

DOI:10.1109/JPHOT.2017.2758820

Manuscript received August 31, 2017; revised September 26, 2017; accepted September 28, 2017. Date of publication October 2, 2017; date of current version October 23, 2017. This work was supported in part by the Conserve & Associates Inc., Taiwan, and in part by the Projects of Ministry of Science and Technology of R.O.C. under Grants MOST105-2221-E-009-085, MOST105-2221-E-009-086, and MOST104-2628-E-009-012-MY3. Corresponding author: Fang-Cheng Lin (e-mail: fclin0210@g2.nctu.edu.tw).

Abstract: Windshield-type vehicle head-up displays (HUDs) are increasingly popular and stepping forward augmented reality; however, the windshield causes an annoying problem—ghost images. By now, the maximal extent of ghost images has not been determined for an HUD with an acceptable legibility. In this paper, to find the quantitative criterion of ghost images regarding subjective perceptions, we first design an HUD using a rotatable aspheric reflector and a wedge-glass windshield. Optical design of the HUD and experimental results of high-quality images are discussed. Next, eight different disparity angles between the primary and ghost images are controllably generated by rotating the aspheric reflector. Based on this HUD platform, human factor experiments utilizing a simulative automotive driving environment are conducted, in which the eight disparity angles are provided to 12 subjects under three ambient contrast ratios (ACRs). The human factor experiments demonstrate that the maximal disparity angles for an acceptable legibility under the ACRs of 3.90, 2.49, and 1.80 are 0.006°, 0.017°, and 0.024°, respectively. These maximal acceptable disparity angles are important references for quantitatively and efficiently evaluating the optomechanical system of an HUD. In addition, they can help to make vehicle laws and regulations for HUDs.

Index Terms: Heads-up displays, ghost reflections, mirror system design, visual comfort.

1. Introduction

Currently, vehicle head-up displays (HUDs) that directly project images onto the windshield are popular in high-end cars, and are also appearing in middle-end and even entry-level cars [1]–[7]. In comparison with an HUD that adopts a pop-up combiner, an HUD that projects onto the windshield provides improved driving safety and more comfortable driving experiences [1], [2]. However, internal and external windshield surfaces generate two virtual images of comparable brightness at different positions, as shown in Fig. 1(a). The virtual image produced by the external surface is called a "ghost image," which disturbs the driver's view of the primary image produced by the internal surface [7]–[10]. A ghost image reduces the legibility of an HUD and hence causes comfort and safety issues. Especially, since vehicle HUDs are now stepping towards augmented

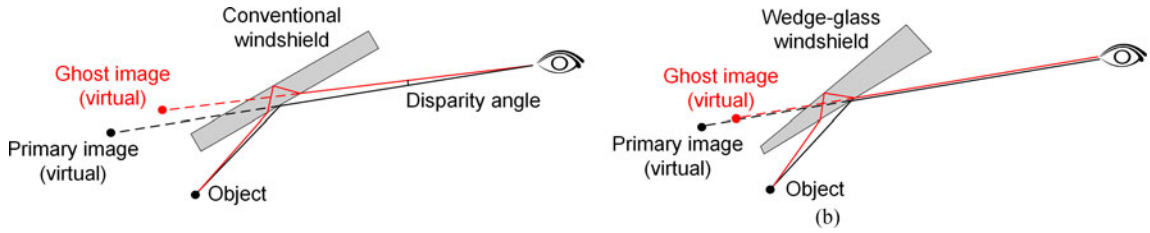

Fig. 1. (a) Ghost image generated by a conventional windshield, where "disparity angle" is also defined. (b) Ghost image eliminated by a wedge-glass windshield.

reality (AR) by displaying increasingly abundant content [5], [11], their legibility should be guaranteed within the acceptable extent of the ghost image.

To solve the ghost image problem, some practical solutions are now being adopted, such as a wedge-glass windshield [8]–[10], which has a small wedge angle between the internal and external windshield surfaces to superimpose the ghost image on the primary image in the driver's line of sight, as shown in Fig. 1(b). However, the ghost image problem is difficult to be solved completely. For instance, mechanical adjustments (e.g., image height tuning), errors of the opto-mechanical system, and changes to the curvature of the windshield may all cause perceptible ghost images to arise again [3], [6]. Therefore, the maximal acceptable extent of a ghost image under which the legibility of an HUD by a driver is acceptable needs to be known as a reference for HUD design [12]–[15]. In addition, laws and regulations for vehicle HUDs are under preparation in many countries, which also call for a quantitative criterion of ghost image for driving safety and visual comfort. As discussed above, the maximal acceptable extent of ghost image is of great importance for HUDs; however, it has been little studied [12]. Moreover, it is quite unpractical to optically treat the windshield, e.g., adding optical coatings or films, because it is usually nondurable against the operating environment of a car, or even illegal in some countries [8]–[10]. Therefore, the brightness ratio between the primary and ghost images is completely determined by the Fresnel equations for reflection and refraction. For example, it is a typical configuration that the refraction index and angle of reflection are respectively 1.5 and 65° for the windshield. In this way, the reflectivity for s-polarized light, which is generated by a liquid crystal display (LCD), can be simply calculated to be approximately 20% at the air-glass interface, then the brightness ratio is fixed at $1 : (1-20\%)^2 = 1 : 0.64$ because the ghost image goes through two extra refractions, compared to the primary image. In case that the brightness ratio is usually unchanged across most of HUDs, the disparity angle between the primary and ghost images, defined in Fig. 1(a), is of primary concern for the ghost image performance.

In this paper, we first design and implement a high-quality HUD using a 1.8-inch LCD, a rotatable aspheric reflector and a wedge-glass windshield. The wedge angle of the windshield can eliminate the ghost image for the initial position of the rotatable aspheric reflector. Next, the aspheric reflector is rotated to adapt to different driver heights. Simultaneously, the elimination condition of the ghost image is broken, and disparity angles between the primary and ghost images corresponding to different rotation angles are calculated. On this HUD platform, human factor experiments are conducted in a simulative automotive driving environment. Twelve subjects evaluate the legibility of HUD images corresponding to the controllable disparity angles under three ambient contrast ratios. Finally, the maximal acceptable values are determined by analyzing the experimental data.

2. HUD Design and Implementation

Currently, the most widely used commercial HUDs adopt projection optics to generate a virtual image on the front of a windshield [3]–[6]. Therefore, to make the human factor investigation of ghost images practical for actual products, we first design and implement a projection-type HUD with a similar architecture. In this section, we will discuss its design method and experimental results to demonstrate the hardware platform for the following human factor investigation. Fig. 2 shows the

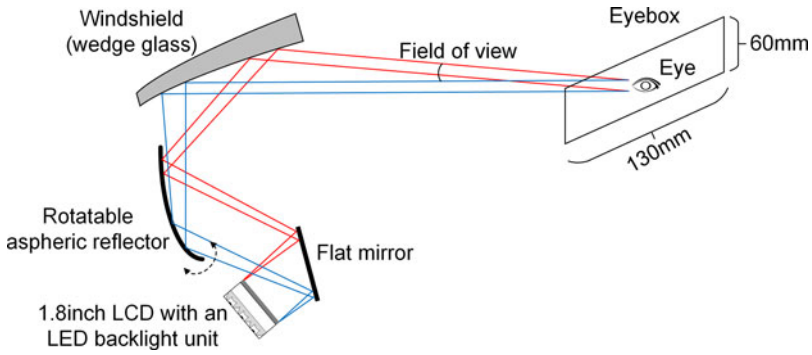

Fig. 2. Optical architecture of the projection-type HUD.

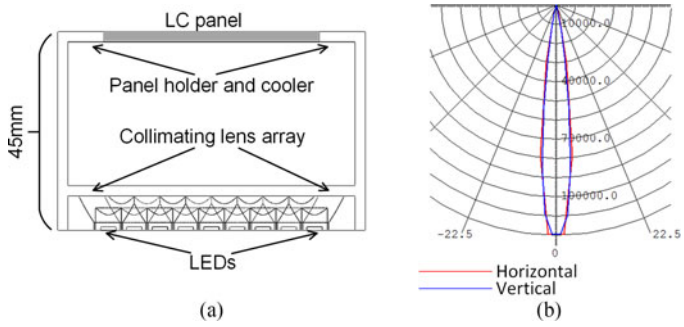

Fig. 3. (a) LED BLU containing 13 LEDs and a collimating lens array for the 1.8-inch LCD (nine LEDs can be seen, while the other four are occluded in the side-view). (b) Angular luminous intensity profile of the central point of the LED BLU in horizontal and vertical directions.

optical architecture of the projection-type HUD, which comprises a 1.8-inch LCD using an LED backlight unit (BLU) and a projection imaging system using a flat mirror, an aspheric reflector, and a wedge-glass windshield. The aspheric reflector can be rotated from $-2°$ to $+2°$ for different driver heights.

2.1 Image Source

An HUD is required to output an image with a luminance as high as approximately 10,000 nits to combat bright sunlight [5]. Moreover, the transmittance of the LC panel and reflectance of the windshield are usually both lower than 10% [16]–[18]. Therefore, the luminance produced by the BLU of the LCD should be extremely high, above 1,000,000 nits. To produce such high luminance, 13 1-Watt LEDs arranged in a "4-5-4" hexagonal array are adopted, and a total-internal-reflection collimating lens is designed to be added onto each LED [19], [20], as shown in Fig. 3(a). Fig. 3(b) shows the simulated angular luminous intensity profile of the central point of the BLU, whose half-value viewing angle is $\pm 8°$. Benefiting from this collimating lens array, on-axis luminance of the BLU is 1,390,000 nits when each LED is fully driven to output a luminous flux of 129 lm. Finally, this BLU is combined with an LC panel that is 1.8 inches (39.8 mm by 22.4 mm) with a resolution of 640 by 480, in compliance with automotive standards, to form an LCD image source.

2.2 Projection Imaging System

In this projection-type HUD, a virtual image of the LCD image source with an image-to-driver distance of 2.5 m and a field of view (FOV) of 6.2° (horizontal) by 4.6° (vertical) is expected along

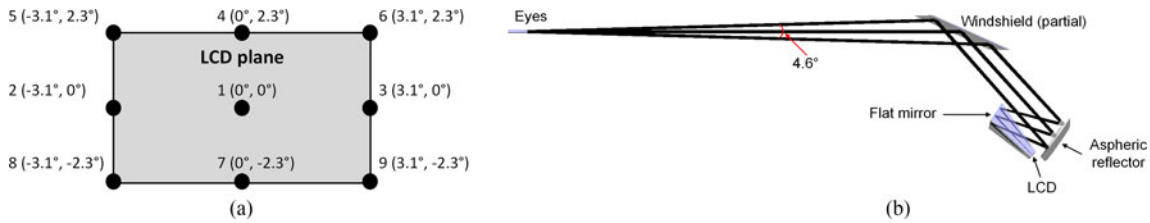

Fig. 4. (a) Nine fields (1 to 9), given by a horizontal angle followed by a vertical angle, and their corresponding positions on the LCD plane. (b) Side view of the light paths in the optimized HUD in LightTools software.

with a 130 mm by 60 mm eyebox, in which either eye of the driver can see a complete image. To fold the light path for the tight space under the dashboard of a car, an off-axis catoptric system is adopted [21]–[25]. Additionally, considering that using more than one curved reflector leads to additional assembly and fabrication costs, we adopt only one curved reflector here, as well as a flat mirror to further fold the light path, as shown in Fig. 2. Corresponding to the aspheric windshield whose curvature radii in the vertical and horizontal directions are 6320 mm and 3550 mm, respectively, the curved reflector has a biconical surface with added x and y polynomial terms, whose sag is given in (1). To provide enough focal power, suppress the aberration, and eliminate the binocular disparity for different rotation positions of the aspheric reflector, the parameters in (1) are carefully determined to build an optimized opto-mechanical system [23]–[25]. To comprehensively investigate the image quality across the FOV of 6.2° by 4.6°, nine representative fields corresponding to nine different positions on the whole LCD plane are selected, as illustrated in Fig. 4(a). Using reversed light paths that are widely adopted in visual system designs, we construct a non-sequential model of the HUD in LightTools software, as shown in Fig. 4(b). Here, light beams of the nine fields are emitted from the eyes with a convergence angle corresponding to a virtual image 2.5 m away, and can all be well focused on the LCD plane, indicating that a clear virtual image with the prescribed FOV can be generated according to the reversibility of light path. We also construct a sequential model in Zemax software. Sagittal and tangent modulation transfer functions (MTFs) corresponding to the two eyes are simulated, as shown in Fig. 5(a). Here, since the pixel size of the LCD is 62 μm, which leads to a cut-off frequency of 8.1 cycle/mm, MTF within this range is of concern. An image of grid wires corresponding to the FOV of 6.2° by 4.6° is simulated to observe the distortion performances, as shown in Fig. 5(b). In consideration of binocular vision, the divergence/convergence diagram is simulated across the FOV, as shown in Fig. 5(c). MTFs higher than 0.6 within the cut-off frequency, a distortion rate smaller than 1%, and a positive vergence smaller than 2 mrad in both vertical and horizontal directions indicate: a high-quality virtual image is produced by the HUD. To investigate the image quality corresponding to different rotation positions of the reflector, MTFs are also simulated for two eyes when the reflector is rotated to $+2°$ and $-2°$, respectively, as shown in Fig. 5(d) and (e). As can be seen, when the reflector is rotated to the maximum angles, the MTFs can still keep higher than 0.5, indicating a consistent image quality within the rotation range. In this way, when the reflector is rotated in the following human experiments, the human perception of the ghost images will not be disturbed by a deteriorating image quality. Such an image quality can be compared well with that of current commercial products [21], [26], [27]. The high image quality will be discussed at the end of this section via experimental results, which demonstrate a reliable hardware platform for human factor investigation.

$$z(x, y) = \frac{c_x x^2 + c_y y^2}{1 + \sqrt{1 - (1 + k_x)c_x^2 x^2 - (1 + k_y)c_y^2 y^2}} + \sum_{i=1}^{N_x} \alpha_i x^i + \sum_{i=1}^{N_y} \beta_i y^i \quad (1)$$

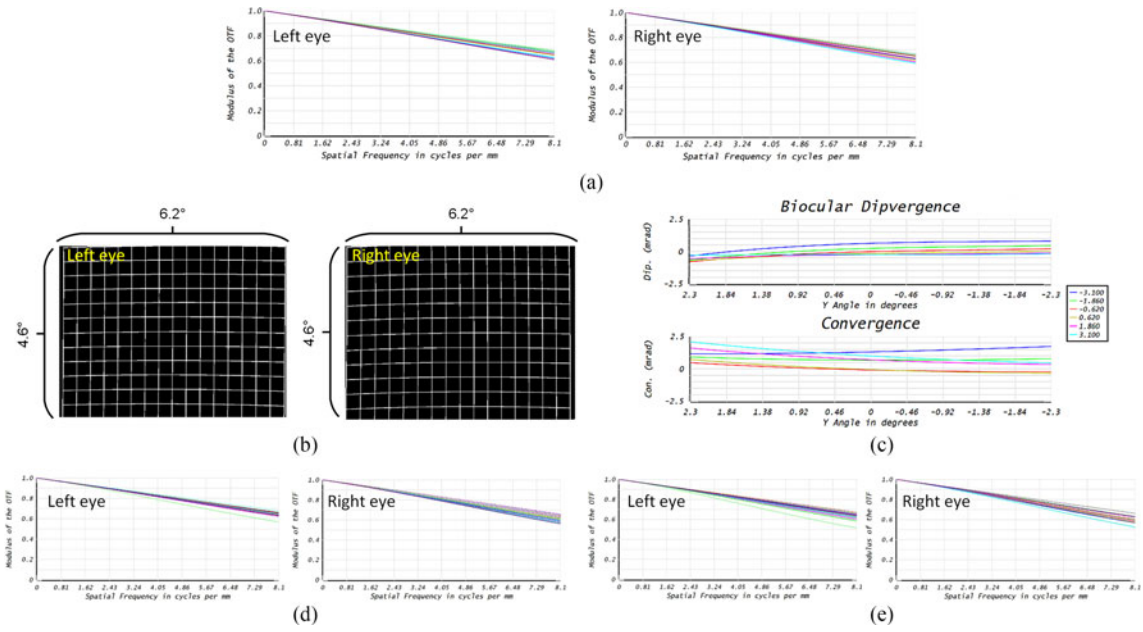

Fig. 5. (a) Sagittal and tangent MTFs of the nine fields corresponding to the two eyes, where 18 colorful lines in each subfigure denote nine fields by two directions; (b) simulated images of grid wires across the FOV corresponding to the two eyes; (c) dipvergence/convergence diagram, where the colorful lines represent different vertical angles from $-2.3°$ to $2.3°$; (d) and (e) sagittal and tangent MTFs of the nine fields corresponding to the two eyes when the reflector is rotated to $+2°$ and $-2°$, respectively.

where c is the reciprocal of the curvature radius, k is the conic constant, α and β are the polynomial terms, and N is the polynomial order. The subscripts x and y denote the x- and y-directions, respectively.

2.3 Ghost Image Elimination

The optimized design of the projection imaging system guarantee that a high-quality primary image is generated by the internal windshield surface. To eliminate the ghost image generated by the external windshield surface, a wedge-glass windshield is adopted. An appropriate wedge angle θ needs to be calculated to position both the primary and ghost images in the driver's line of sight, so that the ghost image can be superimposed on the primary image, as illustrated in Fig. 1(b). To this end, a ray tracing calculation is implemented by Matlab software. In this calculation, as illustrated in Fig. 6, 15 rays are uniformly distributed over a viewing angle of $\pm 5°$ emerge from the central point of the LCD (the object). After being reflected by the designed aspheric reflector and the internal windshield surface (the flat mirror with no optical power is omitted here), these rays propagate into the driver's eye. By tracing the rays backward to a perceived point of origin, a primary image 2.5 m away from the eye can be found, which is guaranteed by the optical design introduced before. Next, by letting the rays transmit through the internal windshield surface, be reflected by the external surface, and transmit through the internal surface again, the ghost image can be calculated similarly.

In the test car, the eyebox inclination is 5°, and the thickness, refraction index (n), and inclination of the windshield are 5.2 mm, 1.5, and 31°, respectively. Here, since the wedge angle is usually very small ($<$1 mrad, [8]–[10]), the thickness variation across the windshield region used for projection is no more than 0.1 mm. Thus, the thickness of the windshield is regarded as a constant in the calculation of the wedge angle. These specifications are used for calculations, and Fig. 6 shows the calculated positions of the primary and ghost images corresponding to different values of wedge

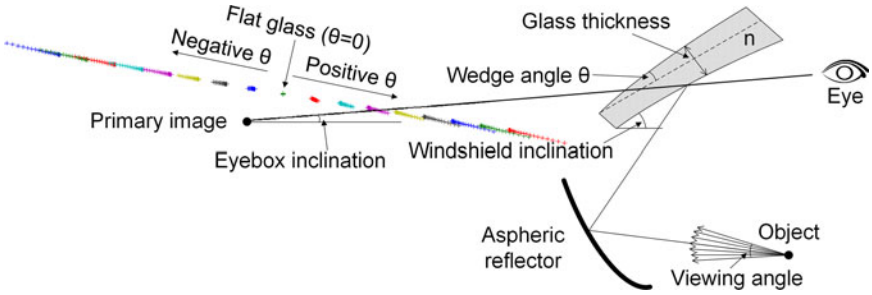

Fig. 6. Positions of the primary and ghost images corresponding to wedge angle θ from -1.6 mrad to 1.6 mrad with a step of 0.2 mrad (the shape of the windshield in this figure corresponds to a positive θ). Scattering points in different colors denote different wedge angles.

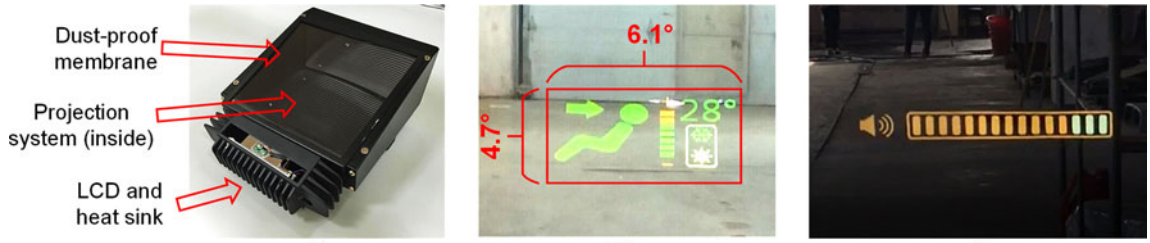

Fig. 7. (a) The HUD system; (b) and (c) captured virtual images.

angle θ. Note that the ghost image is actually a series of scattering points, since extra optical powers are introduced by the thickness of the curved windshield, and a sharp ghost image cannot be generated. By iterative calculations with a precision of 0.01 mrad, the wedge angle θ under which the primary and ghost images can overlap is 0.62 mrad, as shown in Fig. 6. In addition, according to the calculations above, the ghost and primary images can overlap perfectly in only one viewing position; thus, it seems that the ghost image cannot be perfectly eliminated for two eyes simultaneously. Nevertheless, the interpupillary distance is so small compared with the image distance of several meters that the ghost image in the horizontal direction is usually neglected; that is, the ghost image problem is concerned only in the direction perpendicular to the ground [6], [8]–[10].

2.4 Results of the Optimized HUD

The designed HUD is fabricated, as shown in Fig. 7(a), and installed in the test car with the wedge-glass windshield determined in the last section. Through electronic and software development, an actual HUD system is established, whose virtual images, captured by a camera, are shown in Fig. 7(b) and (c). Clear and sharp virtual images without ghost images can be seen. By measuring with a luminance meter and a camera, the full-on luminance is 11,322 nits, the FOV is 6.1° (horizontal) by 4.7° (vertical), and the image-to-driver distance is 2.6 m; these measurements are all in close proximity to the expected specifications.

An HUD with high image quality and no ghost images has been designed and implemented. Experimental results demonstrate a reliable hardware platform on which the following investigation of the maximal acceptable extent of the ghost image can be carried out reasonably and accurately. Additionally, the HUD design with only one curved reflector is superior to that with multiple curved reflectors, since the assembly and fabrication costs can be significantly reduced.

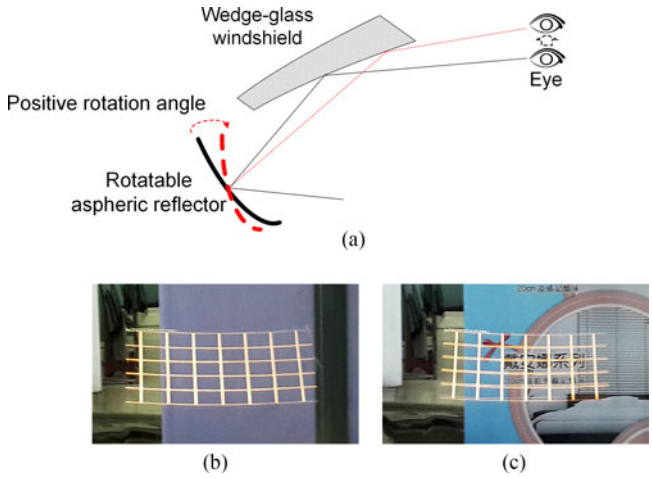

Fig. 8. (a) Image height tuning realized by rotating the aspheric reflector; (b) virtual image without a ghost image, corresponding to the initial position of the reflector; and (c) a virtual image with a perceptible ghost image, corresponding to a rotation angle of $+1.5°$.

3. Human Factor Investigation

3.1 Generation of Controllable Ghost Images

In the HUD designed in-house, as mentioned before, the aspheric reflector can be rotated from $-2°$ to $+2°$ to tune the image height for drivers with different heights, as shown in Fig. 8(a). The corresponding tuning range of image height is ± 56 mm, because the windshield-to-driver distance is 800 mm. Fifteen tuning steps are uniformly distributed from $-2°$ to $+2°$. When the aspheric reflector is at the initial position (rotation angle is 0°), the ray tracing calculation in the last section reveals that the elimination condition of the ghost image can be exactly satisfied. However, when the reflector departs from the initial position, the light path is changed; thus, the elimination condition is broken to a certain degree. For example, from Fig. 8(b) to (c), the reflector is rotated from the initial position to $+1.5°$. Correspondingly, a perceptible ghost image appears.

In current commercial HUDs, the function of driver height adaption is usually realized by rotating the reflector [11], [12], which is the same as the HUD designed in this paper. As discussed above, a perceptible ghost image will be induced when the reflector departs from the initial position because the elimination condition of ghost image is broken to a certain extent. Such a feature is not expected in an HUD; nevertheless, with the aid of this feature, we can control the extent of the ghost image accurately. To be specific, when the aspheric reflector is rotated from $-2°$ to $+2°$, the ray tracing calculation method is used to calculate the primary and ghost image positions. Next, using the definition of disparity angle shown in Fig. 1(a), as the field angle between the primary and ghost images relative to the driver, disparity angles for varying rotation angles can be calculated, as shown in Fig. 9. From Fig. 9, the situations of positive and negative rotation angles are similar; thus, only the positive rotation angles are adopted for the following human factor experiments. In this way, when the aspheric reflector is rotated between 0° and 2° with eight uniform steps, eight disparity angle levels can be produced controllably, as shown in Fig. 9 and Table 1.

3.2 Human Factor Tests

We have established a high-quality HUD with a rotatable reflector, which is able to generate eight different disparity angles between the primary and ghost images. Based on this HUD, human factor experiments are conducted to determine the maximal acceptable disparity angle according to the subjective perceptions of drivers. Twelve subjects aged 23- to 53-years old participate in the human factor experiments to evaluate the ghost image. To simulate an actual driving situation, a simulative

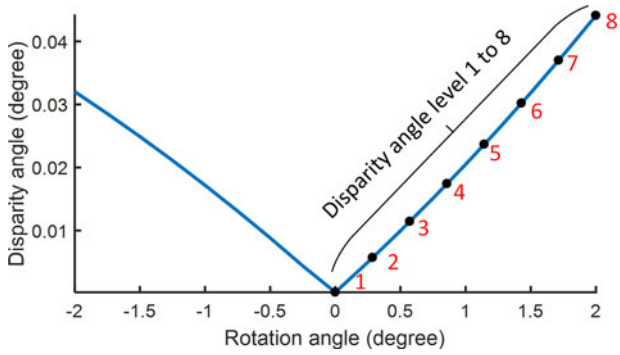

Fig. 9. Disparity angles varying with rotation angles from −2° to 2°; eight disparity-angle levels for the following human factor experiments are marked with black circles.

TABLE 1
Eight Disparity Angle Levels Controllably Produced by Eight Rotation Angles

Disparity angle level	1	2	3	4	5	6	7	8
Rotation angle	0°	+0.29°	+0.57°	+0.86°	+1.14°	+1.43°	+1.71°	+2.00°
Disparity angle	0°	0.006°	0.011°	0.017°	0.024°	0.030°	0.037°	0.044°

Fig. 10. Simulative automotive driving environment projected on a screen 2.5 m away from a subject.

automotive driving environment is projected on a screen 2.5 m away from the driver sitting in the test car, as shown in Fig. 10. The screen with the driving environment projected on it is large enough to fully cover the vision of the driver; hence, the real ambience out of the screen cannot affect the driver's perception. The white grid image in Fig. 8, with different extents of ghost image produced by the rotatable reflector, is shown as the test image. As the test method for see-through HUD images has been little studied, it is difficult to find an acknowledged test chart for it. By considering that we focus on the influence of the ghost image on the legibility in this study, a test image that can fully expose the ghost image is desired. Therefore, the gird image is a good approach because the ghost image only takes place in the vertical direction of the image. If some other charts that do not contain sufficient horizontal lines are used, a bad ghost image performance may be ignored by mistake. In addition, in this study, we focus on the subjective responses to the luminance signals

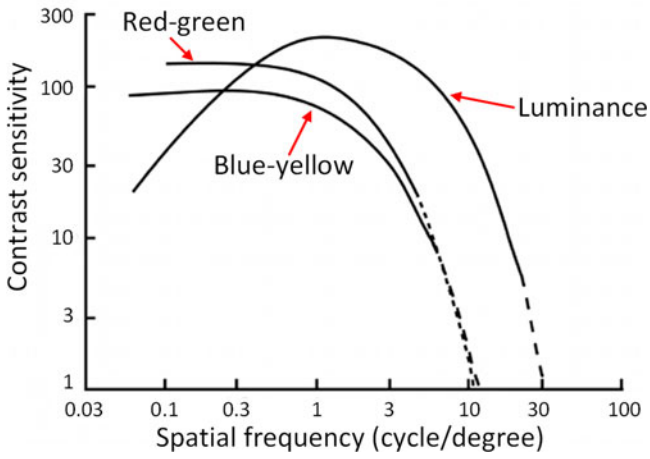

Fig. 11. Contrast sensitivity functions of luminance signals, and red-green and blue-yellow opponent chromatic signals, redrawn from [28]. (Dash lines denote data extrapolated from the experimental data).

TABLE 2
Rating Criteria of Different Ghost Image Performances

Score	Description
1	**Perfect** Legibility — cannot perceive any ghost image at all
2	**High** Legibility — can slightly perceive a ghost image, but reading of the primary image is not affected
3	**Acceptable** Legibility — can perceive a ghost image and can still read the primary image normally
4	**Degraded** Legibility — can clearly perceive a ghost image, and reading of the primary image is mildly affected
5	**Poor** Legibility — can definitely perceive a ghost image and has difficulty in reading the primary image

of HUD images by using this white test image. According to the previous studies of human vision, the human vision system is more sensitive to luminance signals than to chromatic signals when the spatial frequency is high, as shown by the contrast sensitivity functions of luminance and chromatic signals in Fig. 11 [28]. Since a critical ghost image always comes with a high spatial frequency, it is the luminance signals that determine the perception of the ghost images rather than the chromatic signals. In this way, the following results of the maximal acceptable ghost images obtained via the achromatic test image can be directly used for chromatic HUD images because the achromatic luminance signals have a stricter criterion than the chromatic signals do. In the future work, we will do experiments using chromatic images to verify this theoretical discussion.

The drivers' subjective perceptions of the ghost image performance is classified into five rating levels (scores 1 to 5), whose descriptive rating criteria are given in Table 2. Based on the criteria of the ghost image performance, the legibility of the HUD is also classified from "perfect" to "poor," as can be seen in Table 2. First, the 12 subjects evaluate the ghost image corresponding to the rotation angle of 0°. As a result, all the subjects cannot perceive the ghost image definitely, in accordance with the description of score 1 in Table 2, which also reveals that our calculation of the wedge angle that can eliminate the ghost image is completely accurate. Next, the 12 subjects evaluate the ghost image produced by the maximal rotation angle of $+2°$, and they all report that the ghost image performance is so poor that it warrants the rating criterion of score 5. In this way, the subjects have been trained to understand the best (score 1) and the worst (score 5) ghost image performances.

Moreover, by considering that ACR, which is defined in (2), may also influence the perceptibility of ghost images [12], the image luminance is set to 305 nits, 156 nits, and 84 nits, while the ambient luminance is kept at 105 nits, so that three ACRs of 3.90, 2.49, and 1.80 are generated. Here, as mentioned above, the ambience is fully simulated by the images projected on the screen and the real ambience out of the screen cannot affect the driver's perception, thus the luminance from the real ambience, or to say the general lighting, is not considered. The most suitable ACR regarding driving safety and visual comfort is approximately 2:1 according to the previous ergonomic studies for HUDs [11]–[13]. Nevertheless, because the dynamic range of ambient luminance is so large to be from several nits (e.g., in the night) to more than ten thousand nits (e.g., in the bright sunshine), it is difficult to tune an HUD's image luminance to exactly achieve such an ACR all the time. Facing this problem, Gish *et al*. [12] defined the acceptable range of ACR to be 1.15∼4.00, which has been widely acknowledged by the automobile industry. In particular, ACR in a bright and dark ambience tends to be lower and higher, respectively. Therefore, the three ACRs (3.90, 2.49, and 1.80) are utilized in the human factor experiments to cover typical usage scenarios of HUDs. Note that, the legibility of an HUD depends on the perceptibility of the ghost image in our study, as can be seen from Table 2, whereas other factors may also affect the legibility. Nevertheless, in this study, other factors, such as the quality of the primary image, ACR, etc., are all well controlled except that the ghost image extent is variable. In this way, the influence the ghost image has on the legibility can be correctly obtained via the experiments without being disturbed by other factors. In addition, the subjects can score the legibility by just evaluating the ghost image performances. This means the subjective evaluation is easy for the subjects to understand, thus the evaluation results will not vary a lot among different groups of subjects.

$$\text{ACR} = \frac{\text{Image luminance} + \text{Ambient luminance}}{\text{Ambient luminance}} \tag{2}$$

where "image luminance" is the luminance of the image generated by the HUD, and "ambient luminance" is the luminance of the simulative driving environment projected on the screen.

In the human factor experiments, first, under the ACR of 3.90, the eight disparity angles between the primary and ghost images are generated and randomly provided to each subject for him/her to subjectively evaluate. Since different disparity angles are produced by different rotation angles corresponding to different driver heights, during the evaluation, the seat height needs to be adjusted to make the subject always aim his/her sight at the center of the virtual image. Similarly, under the other two ACRs, all the 12 subjects evaluate the eight disparity angles.

After the human factor experiments, the experimental data are analyzed using SPSS software: (i) The p-value in the correlation analysis between the rating score and disparity angle is smaller than 0.001, indicating a significant correlation between the ghost image performance and disparity angle. (ii) The p-value in the correlation analysis between the rating score and the ACR is as small as 0.009, revealing that the ghost image performance is also significantly correlated to ACR. Next, evaluation results of the eight disparity angles under the three ACRs are shown via boxplots in Fig. 12. It can be seen that the ghost image performance becomes worse with increasing disparity angle. Additionally, higher ACR leads to more noticeable ghost images. As discussed in Section 1, the brightness ratio between the primary and ghost images is a fixed value, as about 1:0.64, so a higher ACR directly brings about a higher contrast between the ghost image and the ambience, leading to a more striking ghost image against the ambience. In this study, the legibility of HUD depends on the perceptibility of ghost image because the ACR is controlled within the range for comfortable watching (irrespective of the ghost image performance) in the experiments, and the image quality of the primary image is always high-quality. Therefore, we expect that a higher ACR that brings about a higher contrast between the ghost image and the ambience causes a worse ghost image performance, which has been experimentally verified.

Finally, if an acceptable legibility is desired, the ghost image should perform no worse than what is described as score 3 in Table 2. By selecting the maximal disparity angle level that has a median rating score no larger than 3, the maximal acceptable disparity angle can be determined.

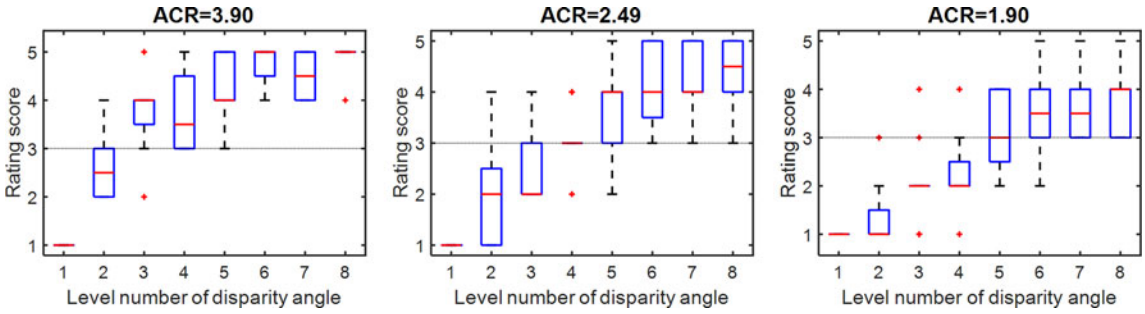

Fig. 12. Boxplots showing evaluation results of the eight levels of disparity angle under three ACRs.

In this way, according to Fig. 12, when the ACRs are 3.90, 2.49 and 1.80, the maximal acceptable disparity angle levels are 2, 4 and 5, respectively. According to Table 1, levels 2, 4 and 5 correspond to the image disparity angles of 0.006°, 0.017°, and 0.024°, respectively. While designing an HUD, the variation of disparity angle can be calculated or simulated corresponding to the tolerances of the opto-mechanical system and the windshield. With the aid of the maximal acceptable disparity angles acquired above, the tolerances can be quantitatively analyzed to guarantee an acceptable legibility.

4. Conclusion

The ghost image is an intrinsic issue in vehicle HUDs that project images onto the windshield. Considering that the maximal acceptable extent of ghost images has not been clearly determined according to the subjective perceptions of drivers, we sought to conduct human factor experiments to investigate the issue in this paper. First, a projection-type HUD using a 1.8-inch LCD, a single aspheric reflector and a wedge-glass windshield was designed and implemented. Imaging performances of the HUD were experimentally verified, including an imperceptible ghost image. This projection-type HUD itself is an advanced optical design example as it uses only one curved reflector to reduce assembly and fabrication costs while achieving an image quality compared well with that of current commercial products using multiple curved reflectors. Next, the aspheric reflector was rotated to generate eight disparity angles between the primary and ghost images, whose values were acquired by a ray tracing calculation. Finally, human factor experiments were conducted, in which the eight disparity angles were provided to 12 subjects for them to evaluate the ghost image performances. Moreover, three different ACRs were considered. The experimental results demonstrated that the ghost image performance strongly depends on both the disparity angle and the ACR. If an acceptable legibility is desired for an HUD, the maximal acceptable disparity angles were found to be 0.006°, 0.017°, and 0.024° under ACRs of 3.90, 2.49 and 1.80, respectively.

With the aid of this conclusion, while designing an HUD, the tolerances of the opto-mechanical system and windshield can be quantitatively analyzed to ensure that the ghost image extent (in terms of disparity angle) does not exceed the proposed maximal values. This analysis can be performed using only numerical calculations or software simulations; that is, HUD design can be more efficient without iteratively developing the expensive aspheric optical system. In addition, laws and regulations for vehicle HUDs are now under preparation in many countries, so this paper can also help to provide a quantitative criterion of ghost images. In consideration of the widespread use of HUDs in cars, especially emerging AR HUDs, driving safety and visual comfort determined by the legibility of HUDs are of increasing importance. Therefore, this study can help to improve driving comfort and safety.

References

[1] J. A. Betancur, G. O.- Gomez, and J. D. Agudelo, "Advances and trends of head-up and head-down display systems in automobiles," *Proc. SPIE*, vol. 9086, 2014, Art. no. 90860E.

[2] Y. C. Liu and M. H. Wen, "Comparison of head-up display (HUD) vs. head-down display (HDD): driving performance of commercial vehicle operators in Taiwan," *Int. J. Human-Comput. Studies*, vol. 61, no. 5, pp. 679—697, 2004.

[3] W. W. Yang, C. H. Chen, and K. T. Luo, "72.2: Compact and high efficiency head-up display for vehicle application," *Soc. Inf. Display Symp. Dig. Tech. Papers*, vol. 43, no. 1, pp. 969–972, 2012.

[4] T.-L. Niu, Y.-C. Hsieh, S. Liao, and H.-P. Kuo, "56.4: A head-up display illuminator design and virtual-image estimation method," *Soc. Inf. Display Symp. Dig. Tech. Papers*, vol. 45, no. 1, pp. 822–825, 2014.

[5] G. Pettitt, J. Ferri, and J. Thompson, "47.1: Invited paper: practical application of TI DLP® technology in the next generation head-up display system," *Soc. Inf. Display Symp. Dig. Tech. Papers*, vol. 46, no. 1, pp. 700–703, 2015.

[6] C.-C. Lee, S.-H. Tsai, C.-C. Kuo, C.-H. Chen, L.-M. Teng, and K.-T. Luo, "P-93: Free ghost image and high transmittance optical thin film beam splitter for head-up display," *Soc. Inf. Display Symp. Dig. Tech. Papers*, vol. 42, no. 1, pp. 1451–1453, 2011.

[7] Y. Takaki *et al.*, "Super multi-view windshield display for long-distance image information presentation," *Opt. Exp.*, vol. 19, no. 2, pp. 704–716, 2011.

[8] J. Hurlbut, D. Cashen, E. Robb, L. L. Spangler, and J. Eckhart, "Next generation PVB interlayer for improved HUD image clarity," *SAE Int. J. Passenger Cars-Mech. Syst.*, vol. 9, no. 1, pp. 360–365, 2016.

[9] R. T. Smith, "Ghost-free automotive head-up display employing a wedged windshield," U.S. Patent 5 013 134, May 7, 1991.

[10] G. E. Freeman, "Windshield for head-up display system," U.S. Patent 5 812 332, Sep. 22, 1998.

[11] J. A. Betancur, J. Villa-Espinal, G. Osorio-Gómez, S. Cuéllar, and D. Suárez, "Research topics and implementation trends on automotive head-up display systems," *Int. J. Interactive Des. Manuf.*, pp. 1–16, 2016.

[12] K. W. Gish and L. Staplin, "Human factors aspects of using head up displays in automobiles: A review of the literature," U.S. Department of Transportation, National Highway Traffic Safety Administration (NHTSA), Interim Rep. no. DOTT HS 808 320, 1995.

[13] S. Smith and S.-H. Fu, "The relationships between automobile head-up display presentation images and drivers' Kansei," *Displays*, vol. 32, no. 2, pp. 58–68, 2011.

[14] S. Höckh, A. Frederiksen, S. Renault, K. Hopf, M. Gilowski, and M. Schell, "Exploring crosstalk perception for stereoscopic 3D head-up displays in a crosstalk simulator," *J. Soc. Inf. Display*, vol. 23, no. 9, pp. 417–428, 2015.

[15] H. Okumura, T. Sasaki, A. Hotta, and K. Shinohara, "Monocular hyper-realistic AR head-up display, " *J. Soc. Inf. Display*, vol. 25, no. 1, pp. 34–43, 2017.

[16] F. Peng, F. Gou, H. Chen, Y. Huang, and S.-T. Wu, "A submillisecond-response liquid crystal for color sequential projection displays," *J. Soc. Inf. Display*, vol. 24, no. 4, pp. 241–245, 2016.

[17] H. Chen *et al.*, "High performance liquid crystal displays with a low dielectric constant material," *Opt. Mater. Exp.*, vol. 4, no. 11, pp. 2262–2273, 2014.

[18] Y.-P. Huang, F.-C. Lin, and H.-P. D. Shieh, "Eco-displays: The color LCD's without color filters and polarizers," *J. Display Technol.*, vol. 7, no. 12, pp. 630–632, 2011.

[19] S. Babadi, R. Ramirez-Iniguez, T. Boutaleb, and T. Mallick, "Performance comparison of a freeform lens and a CDTIRO when combined with an LED," *IEEE Photon. J.*, vol. 9, no. 5, Oct. 2017, Art. no. 6501008.

[20] S. Zhao, K. Wang, F. Chen, D. Wu, and S. Liu, "Lens design of LED searchlight of high brightness and distant spot," *J. Opt. Soc. Amer. A*, vol. 28, no. 5, pp. 815–820, 2011.

[21] B.-H. Kim and S.-C. Park, "Optical system design for a head-up display using aberration analysis of an off-axis two-mirror system," *J. Opt. Soc. Korea*, vol. 20, no. 4, pp. 481–487, 2016.

[22] J. Yang *et al.*, "Method of achieving a wide field-of-view head-mounted display with small distortion," *Opt. Lett.*, vol. 38, no. 12, pp. 2035–2037, 2013.

[23] T. Yang, J. Zhu, W. Hou, and G. Jin, "Design method of freeform off-axis reflective imaging systems with a direct construction process," *Opt. Exp.*, vol. 22, no. 8, pp. 9193–9205, 2014.

[24] T. Gong, G. Jin, and J. Zhu, "Point-by-point design method for mixed-surface-type off-axis reflective imaging systems with spherical, aspheric, and freeform surfaces," *Opt. Exp.*, vol. 25, no. 9, pp. 10663–10676, 2017.

[25] J. Zhu, W. Hou, X. Zhang, and G. Jin, "Design of a low F-number freeform off-axis three-mirror system with rectangular field-of-view," *J. Opt.*, vol. 17, no. 1, 2014, Art. no. 015605.

[26] P. Ott, "Optic design of head-up displays with freeform surfaces specified by NURBS," *Proc. SPIE*, vol. 7100, 2008, Art. no. 71000Y.

[27] L. Bi, X. Fan, K. Jie, T. Teng, H. Ding, and Y. Liu, "Using a head-up display-based steady-state visually evoked potential brain–computer interface to control a simulated vehicle," *IEEE Trans. Intell. Transp. Syst*, vol. 15, no. 3, pp. 959–966, Jun. 2014.

[28] K. T. Mullen, "The contrast sensitivity of human colour vision to red-green and blue-yellow chromatic gratings," *J. Physiol.*, vol. 359, no. 1, pp. 381–400, 1985.